IEEE Access
Multidisciplinary | Rapid Review | Open Access Journal

Received February 16, 2021, accepted March 4, 2021, date of publication March 31, 2021, date of current version April 12, 2021.

Digital Object Identifier 10.1109/ACCESS.2021.3070037

Beam-Reconfigurable Antenna Based on Vector Modulator and Rotman Lens on LTCC

SABIN KUMAR KARKI[1], (Student Member, IEEE), MIKKO VARONEN[2], MIKKO KAUNISTO[2], ARTO RANTALA[2], MARKKU LAHTI[2], ANTTI LAMMINEN[2], JAN HOLMBERG[2], MIKKO KANTANEN[2], JUHA ALA-LAURINAHO[1], AND VILLE VIIKARI[1], (Senior Member, IEEE)

[1]Department of Electronics and Nanosciences, Aalto University School of Electrical Engineering, 00076 Aalto, Finland
[2]VTT Technical Research Centre of Finland, 02044 Espoo, Finland

Corresponding author: Sabin Kumar Karki (sabin.karki@aalto.fi)

This work was supported in part by the Business Finland through 5WAVE Project, and in part by the Academy of Finland through ADENN Project. The work of Sabin Kumar Karki was also supported in part by the Nokia Foundation, and in part by the Walter Ahlström Foundation. The work of Mikko Varonen was also supported by the Academy of Finland Research Fellow Project under Grant 310234.

ABSTRACT A beam-switching array is designed using a 4×6 Rotman lens as a beam-forming network to switch the beam towards $-30°$, $-10°$, $10°$, and $30°$. Six substrate integrated waveguide fed 1×4 microstrip patch arrays are used as the radiating elements. The beam-switching array is designed on the LTCC substrate to operate at 71-76 GHz. In this work, the feasibility of implementing a beam-switching network with a vector modulator (VM) integrated circuit as switching element is studied for the first time. The measured radiation pattern of the beam-switching array with the VM is in line with the simulated radiation pattern. The measured peak realized gain of the beam port 1, 2, 3, and 4 with 3-dB backoff gain of the VM are 17, 17, 17.8, 16.9 dBi at 75 GHz, respectively. In addition, the work demonstrates the possibility of beam-reconfigurability in beam-switching array by simultaneous excitation of the beam ports in optimum phase using the VM. The simultaneous excitation of the adjacent two ports, 1-2, 2-3, and 3-4, steer the beam towards $-19°$, $0°$, and $19°$, respectively, which improves the beam cross-over level. With various combinations of simultaneous excitation, the half power beam-width of the beam-switching array is varied from 17.8° to 75°.

INDEX TERMS Array, beam-switching, beam reconfigurability, microstrip patch antenna, millimeter-wave, Rotman lens, vector modulator.

I. INTRODUCTION

Highly-directive antennas are desired at millimeter-wave frequencies to overcome high path loss and atmospheric attenuation [1]. In addition, the dynamic beam-steering and beam-forming are important features to address the changing environment in mobile communication system. The dynamic beam forming gives control over the directivity, steering angle, and beamwidth of the radiation pattern. The phased array antenna (PAA) is a suitable option for the applications requiring antennas with high-gain and dynamic beam-forming [2]–[4]. However, as the number of the array elements increases, the feeding complexity, the transmission line loss, and the number of active integrated circuits (ICs) increases [5]. Therefore, the thermal management issue becomes critical and the cost of PAA increases substantially.

The beam-switching topology is an alternative solution for high gain applications as it minimizes the number of feed lines and the number of active components [6]–[8]. The beam-switching architecture consists of passive beam-forming networks (BFNs), i.e. Rotman lens, and Butler matrix, and the radiating elements. The number of feeds and their position are determined by the angular coverage, beam-width and the beam cross-over level requirement [9]. The passive beam-steering and beam-forming, i.e. the direction and shape of the beam are predefined based on the feed position, is a major drawback of the beam-switching topology. Typically, only one feed is active at a time to generate a high gain pencil beam towards a specific direction [10].

The beam reconfiguration of an integrated, extended hemispherical lens is demonstrated using the multiple feeds per beam in [11]. The excitation amplitude and phase of the multiple feeds are controlled using a tailored passive BFNs. However, as the number of feed elements increase, the

The associate editor coordinating the review of this manuscript and approving it for publication was Lei Ge.

complexity and losses in the BFN increase and the gain decreases significantly. The beam port excitation phases of a traditional Rotman lens are modified to design the phase-aligned Rotman lens in [12] and wider beams towards a specific direction are produced by simultaneously exciting the phase aligned beam ports.

The selection of a desired feed or the beam switching network is implemented using the RF switches [6], [9], [13], [14]. The high ON-OFF ratio, namely the ratio of RF signal amplitude between the ON and OFF state, of the RF switch ensures the RF signal is present in only desired ports. The solid-state RF switches have the ON-OFF ratio greater than 25 dB [15]. The high ON-OFF ratio ensures that the radiation pattern is not distorted by the RF signal leaking from the unwanted or switched OFF ports. The RF switches suffer high insertion loss at millimeter waves, approx. 2-3 dB per switch [16]. In [17], a 1×16 beam-switching feed network is designed with the SP4T RF switches and the Vivaldi antennas to feed an integrated lens antenna. Based on the transmission line length, the insertion loss of each feed ranges between 7 - 10.5 dB at 71-76 GHz. Similarly, in [14], the total loss of a Rotman lens beam port is more than 10 dB at 28 GHz, and 4.6 dB of the loss is due to two cascaded RF switches.

The high ON-OFF ratio can also be achieved using the beamformer chips that contains amplifiers and phase shifter in each channel [18]. These kind of beamformer chips are widely used in phased array applications to control both amplitude and phase of the radiating elements [3]. A digitally controlled inphase/quadrature (IQ) based vector modulator can provide 360° phase control and 30 dB gain [17], [19]. A beam-switching network can be implemented with the VMs as a switching element by driving the gain of the desired port to maximum while maintaining the remaining channels at the lowest gain.

In this work, for the first time, we aim to replace the RF switch in the beam-switching network with the 4-channel vector modulator IC. The effect of RF signal leaking from undesired channels of the VM on the beam-switching antenna radiation pattern is studied. A beam-switching array based on the 4×6 Rotman lens and six 1×4 substrate-integrated waveguide (SIW) fed patch array is designed and fabricated on the Low Temperature Co-fired Ceramics (LTCC) platform. The beam-switching antenna is designed to operate between 71-76 GHz. The uniform SIW fed 1×4 series array and the vertical transition designed and characterized in [20] are used in this work. The possibility of combining the fixed beams generated by a beam-switching antenna to produce dynamic beams with varying steering angle, directivity, and beamwidth is studied through simulations and measurements. Additionally, the use of vector modulator mitigates the high insertion loss associated with the RF switch.

The paper is organized as follows. In Section 2, the design and simulation results of the Rotman lens based beam-switching array are presented. The use of the vector modulator as switching element is studied in Section 3. Section 4 presents the comparison between the simulation and measurement results of simultaneous excitation of the beam ports for the beam-forming. Finally, the conclusions are made in Section 5.

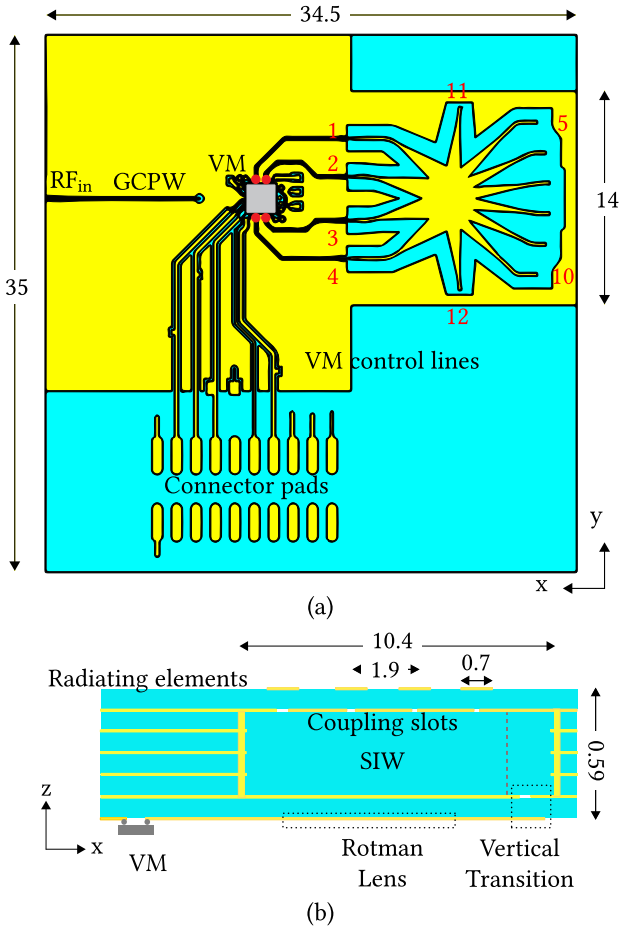

FIGURE 1. (a) Bottom view and (b) cross-section of the Rotman lens based beam-switching array on LTCC detailing the location of VM, Rotman lens, vertical transition, SIW and microstrip patch array. Dimension are in mm.

II. BEAM-SWITCHING ARRAY

The beam-forming network and the array are designed on the 6 tape layer Low Temperature Co-fired Ceramic (LTCC). The Ferro-A6M-E ($\epsilon_r = 5.7$ and $\tan\delta = 0.002$) is used as the substrate. Each dielectric layer of LTCC is 92 µm thick. The thick-film gold material, $\sigma = 7 \times 10^{6}$ S/m, is used as the conductor, and the thickness is 5 µm.

A. ROTMAN LENS

A microstrip Rotman lens is designed with the four beam ports (1-4), six array ports (5-10), and two dummy ports (11-12) as shown in 1 (a). The four beam ports, 1, 2, 3, and 4 are designed to steer the main beam to $-30°$, $-10°$, $10°$, and $30°$, respectively. The focal length of the designed Rotman lens is 3.55 mm, i.e. $1.8\lambda_r$ at the center operating frequency of 73.5 GHz. The separation between the antenna ports (5-10) is 2 mm, i.e $0.5\lambda_0$ at the center operating frequency.

The simulated S-parameters of the beam port 1 and 2 are shown in Fig. 2 (a) and (b), respectively. The S-parameters

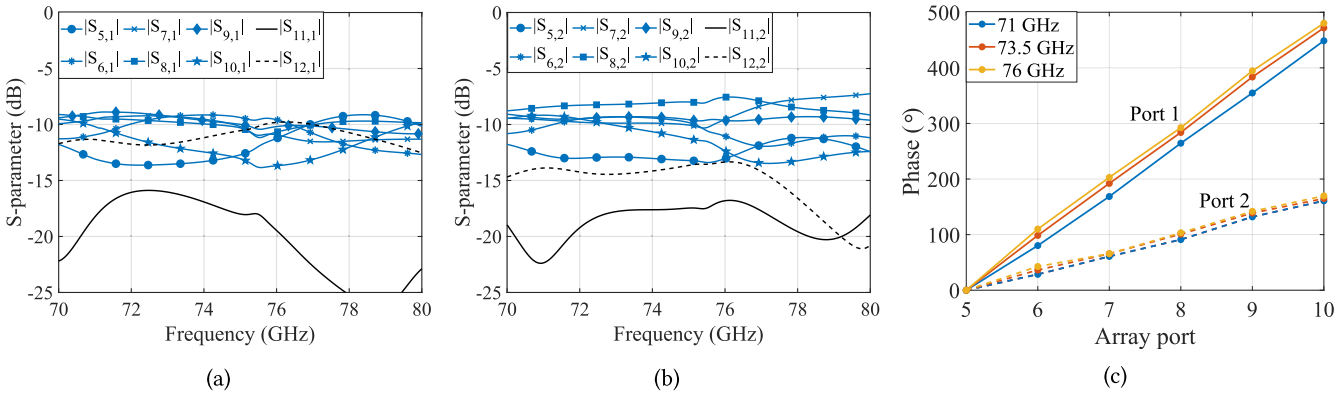

FIGURE 2. Simulated S-parameters of the (a) beam port 1 and (b) beam port 2 and (c) phase distribution across the array ports when beam port 1 (—) and 2 (- -) of the 4 × 6 Rotman lens are excited.

of the Rotman lens are simulated by placing the excitation ports at the begining of the microstrip lines and the array ports are positioned after the vertical transition in the SIW prior to coupling slots, the red line in Fig. 1(b) illustrates the position of the array ports. For both beam ports, 1 and 2, the received amplitude of the array ports at the center are greater than towards the edges. Fig. 2 (c) shows that the progressive phase shifts between the array ports are 30° and 90° when the beam port 1 and 2 are excited, respectively. Due to symmetry of the Rotman lens the S-parameters of port 3 and 4 are the same. The coupling between the beam ports is less than −20 dB for all the beam ports.

B. VERTICAL TRANSITION

In order to make the design compact, the radiating elements are positioned on top of the Rotman lens, at the higher layers of the LTCC as shown in Fig. 1 (b). A transition between a microstrip transmission line and SIW in adjacent LTCC layers is designed by introducing a coupling slot between them. The rectangular slot of 1.8 mm × 0.4 mm is cut from the common ground plane. The transition is designed to operate between 71-76 GHz. A single transition suffers from 0.2-dB loss which is mainly due to reflection and radiation losses. The detail of the design has been published in [20].

C. SERIES ARRAY

A SIW-coupled 1×4 patch antenna array is connected to each array port of the Rotman lens. The width of the SIW is 2 mm and the height is 0.37 mm, i.e., four LTCC tape layers. Four aperture slots on the broader wall of the SIW with varying width are designed to couple equal power to each radiating patch. The width of the four aperture-coupling slots starting from the one close to the vertical transition are 0.1, 0.12, 0.125, and 0.13 mm, respectively. The length of the aperture coupling slots is 1 mm. The coupling slots and the radiating patch are separated by 1.9 mm, i.e. $0.47\lambda_0$ at 73.5 GHz. The length and width of the radiating patch are 0.7 mm and 1 mm, respectively. The E-plane cut of the 1×4 series array radiation pattern is shown in Fig. 3. The simulated directivity of the 1×4 series array is maximum, 11.8 dB, at 75 GHz and it is

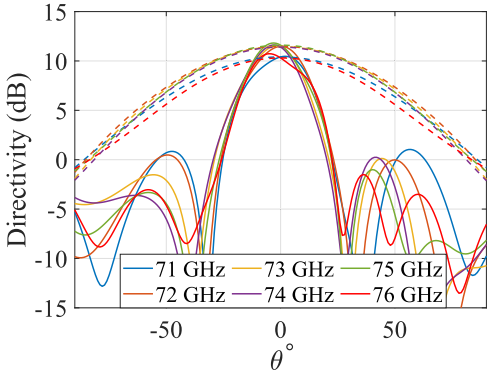

FIGURE 3. Simulated E-/xz-plane (—) and H-/yz-plane (- -) directivity radiation pattern of the SIW fed1 × 4 patch array.

more than 10.5 dB between 71-76 GHz. The detailed design and characterization of the 1×4 series array are detailed in [20].

D. VECTOR MODULATOR

The beam-switching feed network of the Rotman lens consists of grounded co-planar waveguide (GCPW) transmission lines and a 4-channel vector modulator MMIC. A simplified block diagram of the vector modulator is shown in Fig. 4. On-chip power splitting for the four phase shifting elements is implemented using Wilkinson power dividers. The single element TX phase shifter includes a two-stage buffer amplifier in a cascode configuration at the input. The first stage is designed as single-ended to obtain low power consumption. The second stage is a differential one that converts the single-ended mode to a balanced mode for the active vector modulator core that is based on a Cartesian topology. A two-stage differential poly-phase filter is used to generate the required in-phase and quadrature phase (IQ) RF signaling for the variable gain amplifiers. The variable gain amplifiers are realized with two differential Gilbert cells and controlled by on-chip current-steering digital-to-analog converter (DAC) which has eight-bit resolution. The differential output signals of the vector modulator are converted to a single-ended mode by

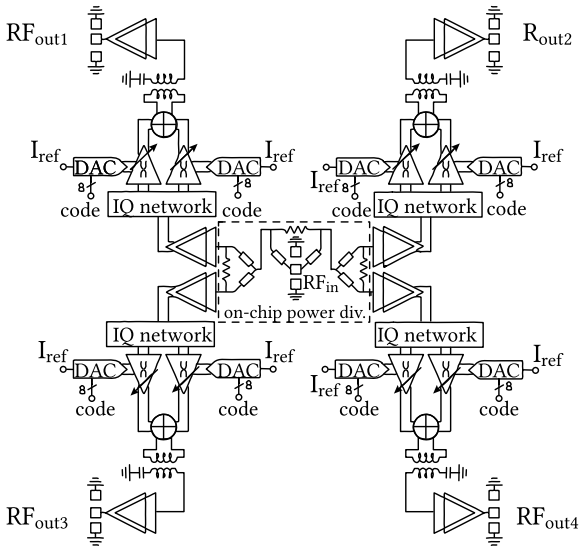

FIGURE 4. Simplified block-diagram of the 4-channel vector modulator MMIC.

a transformer. A two-stage cascode amplifier is used for the final amplifying stage. The 1-dB output compression point for the single-element phase shifter is around 0-dBm power level. The chip is processed in a 0.13 µm SiGe BiCMOS technology. Size of the chip including the pads is 2 mm × 2 mm. The total power consumed by the vector modulator is 0.57 W, 0.142 W per channel.

The vector modulator is measured on-wafer and the $|S_{21}|$ response of a channel is shown in Fig. 5. The measured peak gain of one channel is 24 dB at 75 GHz and 360° phase control can be achieved upto 17 dB gain at 75 GHz.

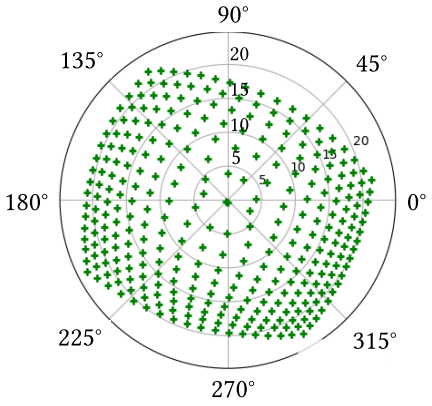

FIGURE 5. Measured $|S_{21}|$ amplitude and phase of a one channel of the VM for various DAC states at 75 GHz.

E. ROTMAN LENS BASED BEAM-SWITCHING ARRAY

The design of the Rotman lens based beam-switching array is shown in Fig. 1. The LTCC module is fed using a 1mm-end-launch connector. The connector is followed by 10 mm and 4.1 mm long grounded co-planar waveguide (GCPW) and stripline, respectively. The stripline is required to access the RF_{in} port of the VM which is located at the center of VM. The VM is attached to LTCC module with flip chip connection using solder bump of 80 µm diameter and 70 µm height. The four beam ports of the Rotman lens are fed with the combination GCPW and microstrip (MS) transmission line. The total length of the transmission lines, sum of GCPW and MS lengths, are 11.3, 8.4, 8.7, and 11.3 mm for beam ports 1, 2, 3, and 4, respectively. The dummy ports of the Rotman lens are terminated with CH02016 50 Ω thin film microwave resistors [21].

The 6 × 4 radiating patch antenna are on the top side as shown in Fig. 1 (b). During simulation studies, the waveguide ports with 50-Ω impedance are used to excite the beam ports at the output of VM, indicated with red circle in Fig. 1. Fig. 6 (a) shows that the simulated reflection coefficient of the beam ports is below −12 dB between 71-76 GHz. The simulated directivity of the beam ports 3 and 2, and 4 and 1 radiating towards ±10° and ±30° are more 16.8 dB and 16.2 dB, respectively between 71-76 GHz. The simulated realized gain peaks at 75 GHz, where the beam ports 2/3 and 1/4 have 11.5 dBi and 10.2 dBi realized gain, respectively. The total efficiency of beam port 1 and 2 are −6.4 dB and −5.8 dB, respectively. The ohmic and dielectric losses are major contributor to the total loss, for example, at 75 GHz, the metallic and dielectric loss of the beam port 2 are 4.3 and 0.7 dB, respectively. The higher loss in the beam port 1 and 4 is mainly due to the longer transmission lines and slightly higher spillover loss coupling to the dummy ports.

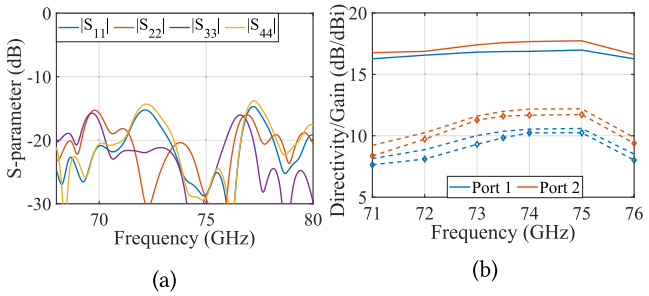

FIGURE 6. Simulated (a) reflection coefficient ($|S_{11}|$) and (b) directivity (—), gain (- -), and realized gain (-⋄-) comparison of the Rotman lens based beam-switching array on LTCC.

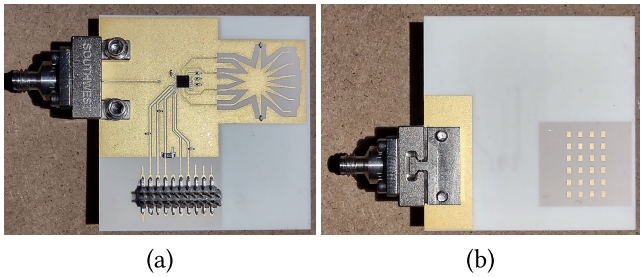

FIGURE 7. (a) Bottom view and (b) top view of the fabricated prototype of the Rotman lens based beam-switching array on LTCC assembled with the end-launch connector.

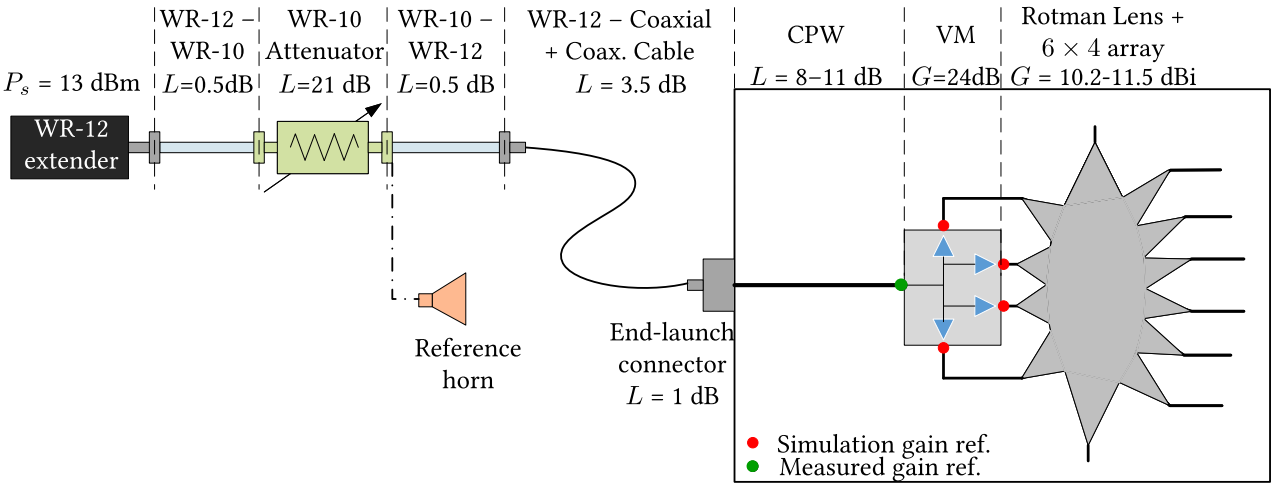

FIGURE 8. Schematic diagram demonstrating the measurement setup and gain estimation of the beam-switching antenna.

The simulated radiation patterns of the beam-switching array are presented along the measured ones in the upcoming sections of the paper.

F. MEASUREMENT SETUP

The fabricated beam-switching antenna assembled with the 4-channel VM and an end-launch connector is shown in Fig. 7. During the measurement, the LTCC antenna module is connected to the WR-12 network analyzer extender using a tunable waveguide attenuator, waveguide-to-coaxial transition (WR-12 to 1-mm coaxial), coaxial cable, and the end-launch connector as shown by the schematic diagram in Fig. 8. The 1-dB output compression point of a single channel of the VM is approx. 0 dBm and the corresponding input power is −24 dBm. However, the output power of the WR-12 extender is 13 dBm. Thus, the tunable attenuator, with 21 dB loss, is connected in the measurement chain to limit the input power to the VM. The loss in the coaxial cable and transition is 3.5 dB [13]. The reflected signal attenuates more than 50 dB in two-way propagation through the attenuator and transmission lines. Since the reflected signal is close to the noise floor of the receiver, the calibration and the S-parameter measurement are not possible.

The radiation pattern and the gain of the designed antenna are measured using the planar near-field measurement technique. The separation between the scanning plane and the LTCC module is 30 mm and the near-field samples are measured at an interval of 1.8 mm. The near-field measurement span is 20 cm which results in valid far-field angular range of ±70°. The gain of the beam-switching array is calculated with the gain comparison method. A reference horn antenna of known gain is measured with same attenuator to estimate the LTCC module gain. The losses in the coaxial-waveguide transition and coaxial cable, 3.5 dB, end-launch connector, 1 dB, and transmission lines between the end-launch connector and the VM, simulated to be 8-11 dB between 71-76 GHz, is compensated during the gain calculation.

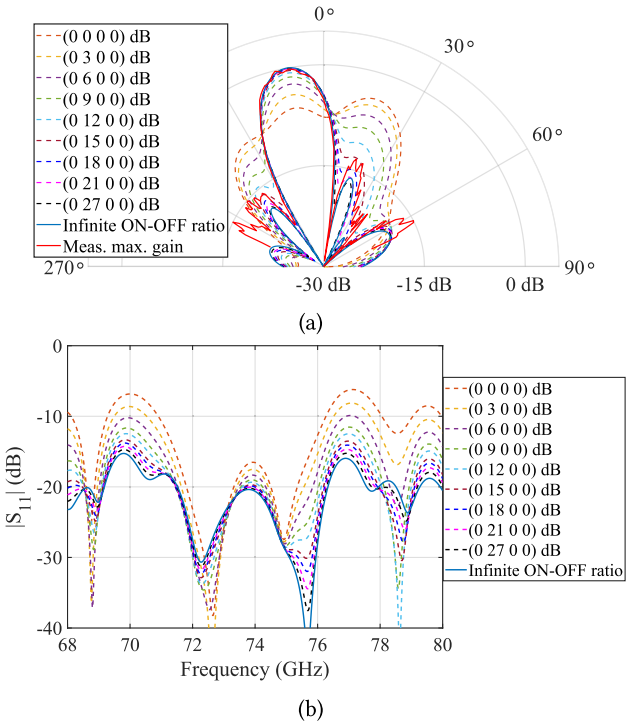

FIGURE 9. (a) Simulated (- -) and measured (—) normalized radiation pattern at 75 GHz, and (b) simulated active reflection coefficient comparison when beam port 2 is amplified and the remaining beam ports are 0-dB gain state.

As shown in Fig. 8, the gain reference point in the simulation and measurement is at the output and input port of the vector modulator, respectively. The use of the attenuator decreases the dynamic range of the measured near-field, therefore, the noise is observed in the measured radiation pattern.

III. VECTOR MODULATOR IC AS RF SWITCH

The output channels of a VM can operate at a number of states between the minimum (OFF) and maximum (ON) gain states. When a VM channel is at the minimum gain or

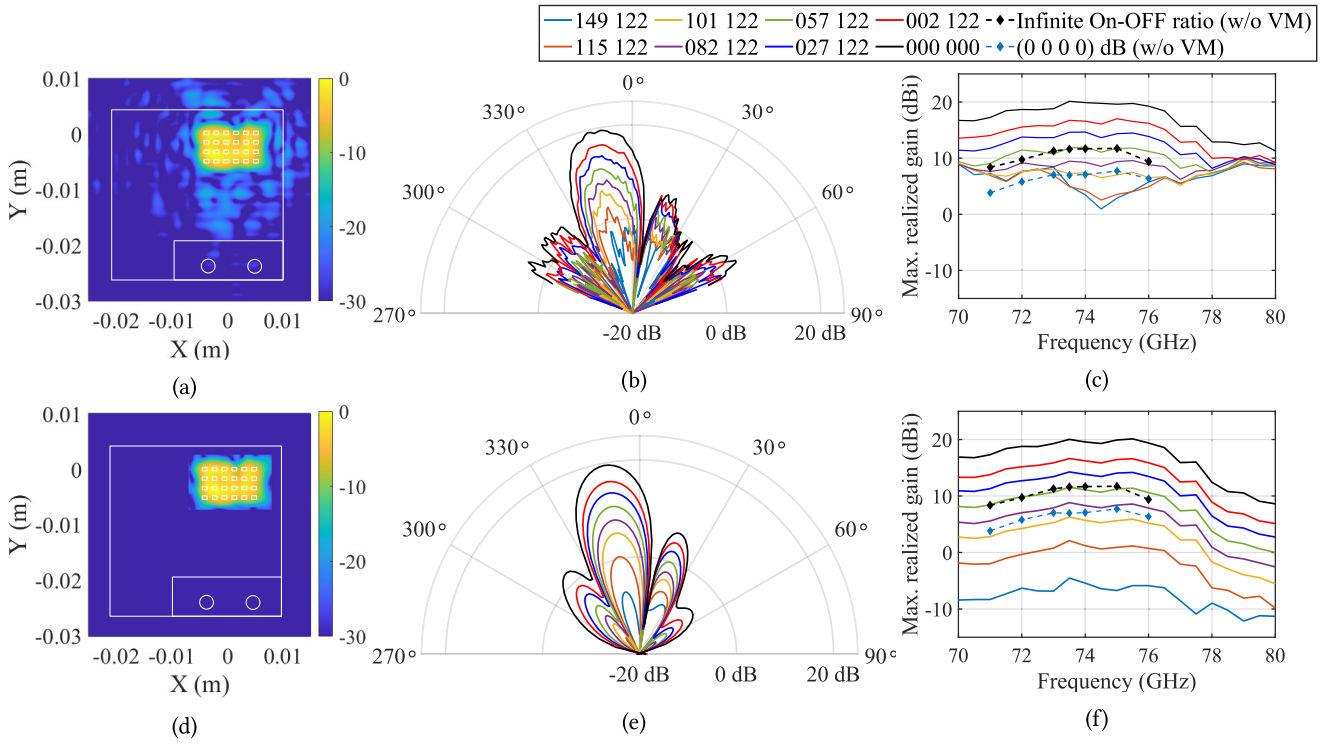

FIGURE 10. Measured (a,d) back-propagated normalized electric field amplitude, (b,e) h-plane radiation pattern cuts at 75 GHz, and (c,f) measured peak realized gain w.r.t. frequency of the beam port 2 with (bottom row) and without (top row) aperture filtering. The measured gain of beam port 2 is varied while remaining beam port 1, 3, and 4 have minimum possible gain, i.e. 149 122. Simulated peak realized gain (-⋄-) without VM are presented in (c) and (f) for comparison.

OFF state, some RF power leaks through the port. The effect of the RF power leaking through the OFF port can be mitigated by increasing the gain of the desired beam port.

In this section, we determine the gain or ON-OFF ratio of the VM required for the Rotman lens based antenna to operate as the beam-switching antenna which produces the pencil beam towards the designed directions. During simulations, the beam ports 1, 3, and 4 of the Rotman lens are excited with the minimum, 0-dB, amplitude while the excitation amplitude of the beam port 2 is increased from 0 - 27 dB. The radiation pattern with the varying excitation amplitude at the beam port 2 is compared to the ideal radiation pattern, i.e. when beam port 2 is excited with infinite ON-OFF ratio, see Fig. 9 (a). In Fig. 9 (a), the simulated directivity radiation patterns are normalized with respect to the peak directivity of the beam port 2 with infinite ON-OFF ratio and the measured realized gain radiation pattern is normalized with respect to its peak. When all the beam ports of the Rotman lens are equally excited, a very wide and asymmetrical beam is formed. The beam is asymmetrical because the path length of each beam port from the vector modulator to input of the Rotman lens is different. Therefore, the excitation phases of the beam ports are not the same and the superposition of their far-fields form the asymmetrical radiation pattern. With the increasing beam port 2 excitation amplitude, the directivity improves, the side lobe level decreases, and the radiation pattern begins to resemble more like an ideal radiation pattern, i.e. beam-switching scenario. The simulation study shows that the gain or ON-OFF ratio greater than 21 dB limits the peak directivity difference below 0.1 dB and SLL level difference at 1-dB level.

The simulated active reflection coefficient of the beam port 2 is presented in Fig. 9 (b). When all the beam ports are active, (0 0 0 0) dB, the active reflection coefficient differs with the beam-switching case. However, with increasing excitation amplitude the active reflection coefficient of the beam port 2 matches the reflection coefficient of the beam-switching case. The simulated active reflection coefficient is below −10 dB for all the excitation amplitudes as shown in Fig. 9 (b).

The measured realized gain radiation pattern of the beam port 2 with varying VM gain is shown in Fig. 10 (b). For a single channel of the VM, the DAC states 149 122 and 000 000 represent the minimum and maximum gain states, respectively. As expected, with the higher gain at the beam port 2, the SLL decreases and the radiation pattern resembles the ideal radiation pattern of the beam port 2. The simulated and measured normalized radiation pattern comparison in Fig. 9 (a) shows that the main lobe is steered towards the same direction, −10°, and the HPBWs are 18°, respectively. At 75 GHz, the simulated and measured SLL are 16.8 dB and 13.75 dB, respectively.

The measured radiation pattern shown in Fig. 10 (b) have noise and at the lowest gain states, 149 122 and 115 122,

the measured radiation patterns do not ressemble the simulated radiation pattern. The ripples in the radiation patterns are mainly caused by: the spurious radiation from LTCC module, and the limited near-field dynamic range due to use of the attenuator. The back-propagated electric field at the radiating aperture of the LTCC shown in Fig. 10 (a) demonstrates that there are radiating fields present outside the 6×4 patch antenna array. The amplitude of spurious electric fields is constant for all the gain states, which suggests that the leakage happens prior to the VM. As the VM gain increases, the patch array amplitude increases and the radiation pattern starts to behave as the simulations. The undesired radiation sources are filtered as shown in Fig. 10 (d) and the filtered aperture fields are transformed into the far-field radiation pattern in Fig. 10 (e). The filtered radiation patterns do not have ripples, and at the lower gain states the measured radiation patterns are in good agreement with the simulations. The filtered peak realized gain, in Fig. 10 (f), has larger gain range, following the gain difference between the lowest and highest gain states of the VM, as compared to unfiltered gain in Fig. 10 (c). The average filtered gain range between 71 - 76 GHz is more than 25.5 dB. Based on simulations, the expected gain improvement towards the specific direction, $-10°$, equal to the VM gain, i.e. 24 dB. The filtered peak gain shows that the gain of the VM is close to expected.

The simulation and measurement gain reference point is shown in Fig. 8. The losses in WR12-coaxial transition, coaxial cable, end-launch connector and GCPW has been compensated in the measurement results. The expected realized gain of the LTCC module, when the beam port 2 is only excited with maximum VM gain, is approx. 35.5 dBi, 24 dB VM gain and 11.5 dBi LTCC antenna gain, at 75 GHz. However, at 75 GHz, the measured peak gain is 20 dBi. Similarly, the difference between the simulated and measured realized gain of the beam-switching antenna, when all ports are equally excited, (0 0 0 0) dB, is approx. 14-15 dB, see Fig. 10 (f). The RF signal leakage between the end-launch connector and the VM is a possible reason for the difference between the simulated and measured realized gain. Furthermore, the height of the solder bump used in the flip chip connection of the VM were smaller than expected which could degrade the impedance matching of the flipchip. The vector modulator is integrated with the antenna, therefore the differentiation between the antenna and beam-switching network efficiency is not possible.

When the VM gain is maximum, the 360° phase control is not possible, see Fig. 5. Therefore, the gain is lowered by 3 dB, to achieve wide phase control, approx. 260°, at the same amplitude level, which is adequate for this work. Further wider phase control can be achieved by lowering the VM gain as shown in Fig. 5. The measured normalized realized gain pattern of all the beam ports with the backoff gain are in close agreement with the simulated ideal radiation pattern, see Fig. 11. Both the simulated and measured realized gain of the beam ports are normalized with respect to the peak realized gain of the beam port 2. The comparison between

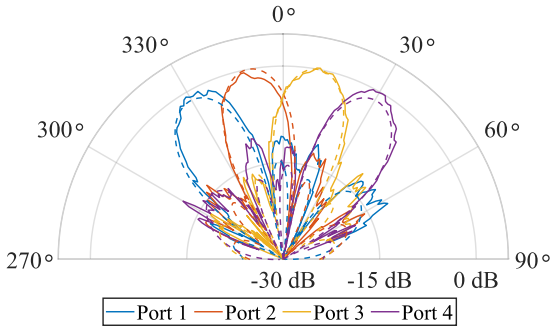

FIGURE 11. Normalized radiation pattern comparison between the beam-switching simulation (- -) and (002 122) gain measurement (—) of 4 beam ports.

the simulated and measured far-field properties of the four beam ports are detailed in Table 1. The measured scan loss of the beam-switching array is less than 0.8 dB conforming to the simulation results. The minor difference between the simulation and measurement results in beam angle and first SLL is caused by the noisy far-field radiation pattern due to leaking radiation and the limited near-field dynamic range.

TABLE 1. Comparison between the simulated and measured far-field properties of the LTCC module.

Port	Angle (°)		HPBW (°)		Scan loss (dB)		First SLL (dB)	
	Sim.	Mea.	Sim.	Mea.	Sim.	Mea.	Sim.	Mea.
1	−30	−31	19.5	19	1.5	0.8	−13.6	−11
2	−10	−12	18	17	0	0.2	−16.6	−13
3	10	11	18	18	0	0	−16.9	−12.5
4	30	30	19.5	19	1.5	0.2	−13.2	−12.4

The close agreement between the simulated and measured radiation pattern validates the idea of using the high-gain vector modulator as the switching element in the beamforming network. Though, the measured realized gain is substantially lower than the expected gain, the use of vector modulator still improves the measured gain by approx. 8.5 dB compared to the simualations, without VM, see Fig. 10 (c) and (f). Furthermore, it is important to notice that additional 2-3 dB insertion loss due to RF-switches has been avoided by using VM as the switching element.

IV. BEAM RE-CONFIGURABILITY

In this section, more than one beam ports are excited at the same time. When the multiple beam ports are excited, the resulting radiation pattern is the vector sum of the excited beam port radiation patterns. The radiation pattern of the beam ports can be added constructively towards a specific direction by appropriately phasing the beam ports. The combination of the excited beam ports can be selected based on the required radiation pattern.

A. TWO-PORT COMBINATION

In this subsection, the two beam ports of the Rotman lens are simultaneously excited with equal amplitude. The I and

TABLE 2. Comparison between the simulated and measured (in bracket) excitation amplitude, phase and far-field properties of the various adjacent beam combinations.

Combination	Port 1		Port 2		Port 3		Port 4		Angle (°)	HPBW (°)	First SLL (dB)
	Amp.	Phase (°)	Amp.	Phase (°)	Amp.	Phase (°)	Amp.	Phase (°)			
Port 1 & 2	1	0	1	355 (340)	0	0	0	0	−19 (−21)	25 (21)	−16.1 (−16.5)
Port 2 & 3	0	0	1	0 (0)	1	55 (65)	0	0	0 (2)	27.5 (25)	−19.6 (−15)
Port 3 & 4	0	0	0	0 (0)	1	0	1	260 (270)	19 (21)	25 (22)	-16.4 (-15.5)
Port 1 & 2 & 3	1	0 (0)	1	20 (350)	1	55 (45)	0	0	−9 (−22)	53 (51)	−10.5 (-13.5)
Port 2 & 3 & 4	0	0	1	0 (0)	1	280 (310)	1	340(340)	−5 (−5)	53 (52)	−12 (−13)
Port 1 & 2 & 3 & 4	1	0 (0)	1	260 (260)	1	150(120)	1	215(185)	−2(−22)	75	−13.1 (−13.5)

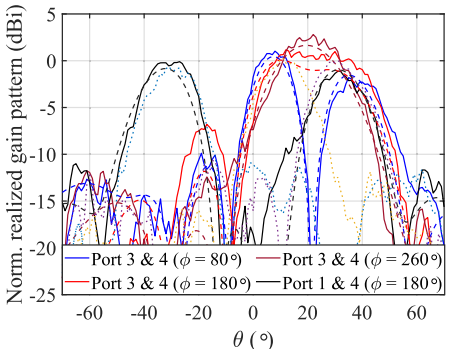

FIGURE 12. Simulated (- -) and measured (—) normalized radiation pattern comparison when two beam ports are simultaneously excited with the appropriate phase. The measured pattern (· · ·) of combining beam port 1, 3, and 4 are also plotted for reference.

Q control vectors are varied only to change the phase while maintaining the constant gain. The remaining beam ports are assigned the lowest gain.

The combination of the distant 2 beam ports, for example, beam port 1 and 4, will result in a multi-beam radiation pattern with main lobes towards the direction −30° and 30°, see Fig. 12. The 180° phase difference, ϕ, between beam ports 1 and 4 help to reduce the SLL. The adjacent beams, like the beam port 3 and 4, can be excited with appropriate ϕ to generate: (1) a multi-beam radiation pattern, with $\phi = 80°$, (2) a flat-top shaped beam with wide angular coverage, with $\phi = 180°$, and (3) a single directive beam between the combining beams, with $\phi = 260°$.

The possible adjacent two port combinations for the four beam ports are 1-2, 2-3, and 3-4. The phase difference between the beam ports 1-2, 2-3, and 3-4 are optimized to steer the main beam towards −19°, 0°, and 19°, respectively. The phase difference between the combining ports used in the simulation and measurement are in close agreement with each other, see Table 2. Figure 13 (a) shows that the simulated and measured realized gain radiation patterns follow each other. The simulated directivity of the beam port combination 1-2, 2-3, and 3-4 are 16.2 dB, 15.8 dB and 16.2 dB, respectively, which are lower compared to the individual beam ports directivity. Similarly, the HPBW of the combination beams are larger than that of the individual beam ports. The simultaneous excitation of the adjacent ports as demonstrated in Fig. 13 (a), can improve the beam cross-over levels. For example, the beam cross-over level of the beam port 2 and 3

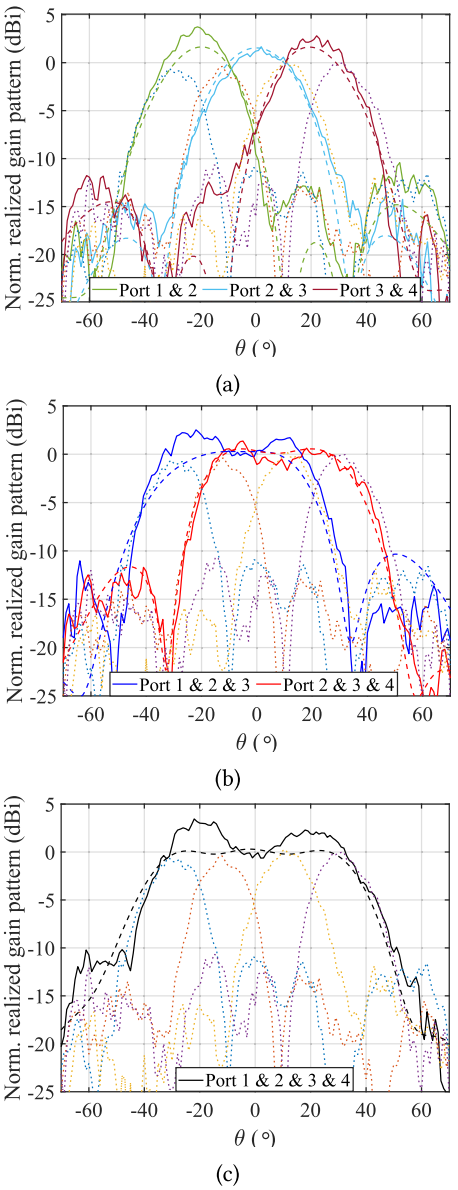

FIGURE 13. Comparison between the simulated (- -) and measured (—) normalized radiation patterns, when (a) two, (b) three, and (c) four adjacent beam ports are simultaneously excited with the appropriate phase. The individually measured beams (· · ·) are plotted for reference.

is −5.4 dB towards the boresight direction. The simultaneous excitation of port 2 and 3 creates beam towards boresight with approx. 6 dB higher gain than the beam cross-over level.

B. WIDE BEAMS

In this subsection, three and four adjacent beam ports are simultaneously excited with equal amplitude, i.e. equivalent to 002 122, and appropriate phase to form wide beams. The details of excitation amplitudes and phases are in Table 2. Fig. 13 (b), (c), and Table 2 show that the measured radiation pattern of three and four port combinations are in consonance with the simulation results. Both the three port combinations, 1-2-3 and 2-3-4, have 13.1 dB simulated directivity and the main lobe is directed towards $-9°$ and $-5°$, respectively. The simulated directivity of the four port combination, 1-2-3-4, is 12 dB and the main beam is pointed towards $-2°$. The HPBW of the beam port combinations 1-2-3, 2-3-4, and 1-2-3-4 are 53.1°, 51.7°, and 75°, respectively. The comparison between the various combinations show that as the number of combining ports increase, the directivity decreases and the HPBW increases. Though, the beam combination reduces the directivity of the resulting beam, the peak realized gains are comparable due to the additional VM gain of the combining beam ports that adds constructively in the far-field to form wider beams.

The simulated and measured normalized peak realized gain performance of the different beam combinations are shown in Fig. 14 (a) and (b), respectively. The excitation phases for various beam combination illustrated in Table 2 are optimized for 75 GHz. Figure 14 shows that the beam reconfigurability can be achieved for wide frequency band. The results are normalized with respect to the peak gain of the beam port 2 when other beam ports are at the low gain state. The normalized simulation and measurement results for the one, two, and three beam-port excitations are in close agreement with each other. Some minor differences between simulation and measurement can be associated with the ripples in radiation pattern due to RF leakage and limited dynamic range.

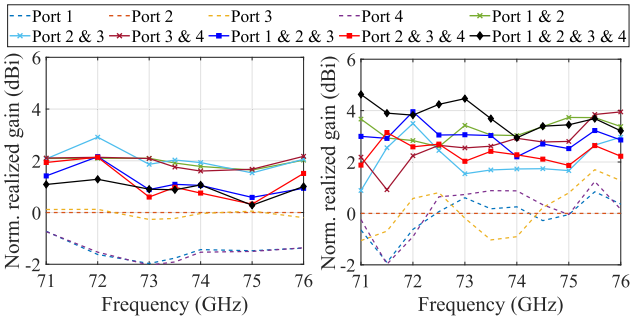

FIGURE 14. Normalized (a) simulated and (b) measured realized peak gain response of the beam-reconfigurable array for various beam combinations. The gains are normalized against port 2 single beam case.

V. CONCLUSION

In this paper, a beam-switching antenna array is designed based on the 4×6 Rotman lens to steer the main beam towards $\pm30°$ and $\pm10°$ at 71-76 GHz. The antenna array is implemented in a 6-layer LTCC platform. The beam-switching network is implemented using a 4-channel vector modulator instead of a traditional RF switch. The simulation and measurement study suggest that a VM with the sufficient gain, e.g., more than 24 dB in this particular case, can be used to implement the beam-switching network. The good agreement between the simulated and measured HPBW, beam steering angle, and SLL of all the beam ports justify the feasibility of the VM.

The use of the vector modulator in the beam-switching network mitigates the high insertion loss of a traditional RF switch. Furthermore, the use of vector modulator enables the beam reconfigurability for the beam-switching antenna. The high gain pencil beams and reconfigurable wide beams of the beam-switching array are demonstrated through the simulations and measurements.

ACKNOWLEDGMENT

The authors wish to thank Infineon Technologies GmbH, Villach, Austria for providing MMIC manufacturing. Especially, support of Samo Vehovc and Johann Wuertele, are highly appreciated.

REFERENCES

[1] T. S. Rappaport, S. Sun, R. Mayzus, H. Zhao, Y. Azar, K. Wang, G. N. Wong, J. K. Schulz, M. Samimi, and F. Gutierrez, "Millimeter wave mobile communications for 5G cellular: It will work!" *IEEE Access*, vol. 1, pp. 335–349, 2013.

[2] R. Valkonen, "Compact 28-GHz phased array antenna for 5G access," in *IEEE MTT-S Int. Microw. Symp. Dig.*, Jun. 2018, pp. 1334–1337.

[3] K. Kibaroglu, M. Sayginer, T. Phelps, and G. M. Rebeiz, "A 64-element 28-GHz phased-array transceiver with 52-dBm EIRP and 8–12-Gb/s 5G link at 300 meters without any calibration," *IEEE Trans. Microw. Theory Techn.*, vol. 66, no. 12, pp. 5796–5811, Dec. 2018.

[4] M. K. Leino, R. Montoya Moreno, J. Ala-Laurinaho, R. Valkonen, and V. Viikari, "Waveguide-based phased array with integrated element-specific electronics for 28 GHz," *IEEE Access*, vol. 7, pp. 90045–90054, 2019.

[5] G. Gultepe, S. Zihir, T. Kanar, and G. M. Rebeiz, "A dual-polarized 1024-element Ku-band SATCOM transmit phased-array with ±70° scan and 43.5 dBW EIRP," in *IEEE MTT-S Int. Microw. Symp. Dig.*, Aug. 2020, pp. 837–840.

[6] A. Lamminen, J. Säily, M. Kaunisto, M. Pokorný, J. Aurinsalo, and Z. Raida, "Gain enhanced millimetre-wave beam-switching rotman lens antenna designs on LCP," in *Proc. 11th Eur. Conf. Antennas Propag. (EUCAP)*, Mar. 2017, pp. 2781–2785.

[7] J.-W. Lian, Y.-L. Ban, Q.-L. Yang, B. Fu, Z.-F. Yu, and L.-K. Sun, "Planar millimeter-wave 2-D beam-scanning multibeam array antenna fed by compact SIW beam-forming network," *IEEE Trans. Antennas Propag.*, vol. 66, no. 3, pp. 1299–1310, Mar. 2018.

[8] J. Ala-Laurinaho, J. Aurinsalo, A. Karttunen, M. Kaunisto, A. Lamminen, J. Nurmiharju, A. V. Räisänen, J. Säily, and P. Wainio, "2-D beam-steerable integrated lens antenna system for 5G *E*-band access and backhaul," *IEEE Trans. Microw. Theory Techn.*, vol. 64, no. 7, pp. 2244–2255, Jul. 2016.

[9] F. Foglia Manzillo, M. Śmierzchalski, L. Le Coq, M. Ettorre, J. Aurinsalo, K. T. Kautio, M. S. Lahti, A. E. I. Lamminen, J. Säily, and R. Sauleau, "A wide-angle scanning switched-beam antenna system in LTCC technology with high beam crossing levels for V-band communications," *IEEE Trans. Antennas Propag.*, vol. 67, no. 1, pp. 541–553, Jan. 2019.

[10] Y. J. Cheng, W. Hong, K. Wu, Z. Q. Kuai, C. Yu, J. X. Chen, J. Y. Zhou, and H. J. Tang, "Substrate integrated waveguide (SIW) Rotman lens and its Ka-band multibeam array antenna applications," *IEEE Trans. Antennas Propag.*, vol. 56, no. 8, pp. 2504–2513, Aug. 2008.

[11] N. T. Nguyen, R. Sauleau, M. Ettorre, and L. L. Coq, "Focal array fed dielectric lenses: An attractive solution for beam reconfiguration at millimeter waves," *IEEE Trans. Antennas Propag.*, vol. 59, no. 6, pp. 2152–2159, Jun. 2011.

[12] Y. Zhang, S. Christie, V. Fusco, R. Cahill, G. Goussetis, and D. Linton, "Reconfigurable beam forming using phase-aligned Rotman lens," *IET Microw. Antennas Propaga.*, vol. 6, no. 3, pp. 326–330, Feb. 2012.
[13] A. E. I. Lamminen, S. K. Karki, A. Karttunen, M. Kaunisto, J. Säily, M. Lahdes, J. Ala-Laurinaho, and V. Viikari, "Beam-switching dual-spherical lens antenna with low scan loss at 71–76 GHz," *IEEE Antennas Wireless Propag. Lett.*, vol. 17, no. 10, pp. 1871–1875, Oct. 2018.
[14] M. Heino, C. Icheln, J. Haarla, and K. Haneda, "PCB-based design of a beamsteerable array with high-gain antennas and a Rotman lens at 28 GHz," *IEEE Antennas Wireless Propag. Lett.*, vol. 19, no. 10, pp. 1754–1758, Oct. 2020.
[15] C. W. Byeon and C. S. Park, "Design and analysis of the millimeter-wave SPDT switch for TDD applications," *IEEE Trans. Microw. Theory Techn.*, vol. 61, no. 8, pp. 2858–2864, Aug. 2013.
[16] T. Semiconductor. *70-90 GHz SP4T Switch Flip Chip, TriQuint Semiconductor*. Accessed: Nov. 2009. [Online]. Available: https://datasheetspdf.com/pdf-file/720912/TriQuintSemiconductor/TGS4306-FC/1
[17] M. Kantanen, J. Holmberg, M. Varonen, and A. Rantala, "Digitally controlled vector modulator SiGe MMIC for millimeter-wave phased array applications," in *Proc. 11th German Microw. Conf. (GeMiC)*, Mar. 2018, pp. 51–54.
[18] S. Zihir, O. D. Gurbuz, A. Kar-Roy, S. Raman, and G. M. Rebeiz, "60-GHz 64- and 256-elements wafer-scale phased-array transmitters using full-reticle and subreticle stitching techniques," *IEEE Trans. Microw. Theory Techn.*, vol. 64, no. 12, pp. 4701–4719, Dec. 2016.
[19] M. Kantanen, J. Holmberg, and T. Karttaavi, "Two-way vector modulator SiGe MMIC for millimeter-wave phased array applications," in *Proc. Global Symp. Millimeter-Waves (GSMM)*, May 2015, pp. 1–3.
[20] S. K. Karki, J. Ala-Laurinaho, J. Zheng, M. Lahti, and V. Viikari, "Millimeter-wave stepped series array with LTCC," in *Proc. 49th Eur. Microw. Conf. (EuMC)*, Oct. 2019, pp. 956–959.
[21] V. Sfernice, *High Frequency 70 GHz Thin Film Chip Resistor*. Vishay. Accessed: Jan. 2021. [Online]. Available: https://www.vishay.com/docs/53014/ch.pdf

SABIN KUMAR KARKI (Student Member, IEEE) was born in Kathmandu, Nepal, in 1988. He received the B.E. degree in electronics and communication engineering from Tribhuwan University, Nepal, in 2010, and the M.Sc.(Tech) degree in radio science and engineering from Aalto University, Finland, in 2016, where he is currently pursuing the Ph.D. degree in radio engineering.

In 2016, he joined the Department of Electronics and Nanoengineering, Aalto University, as a Research Assistant. His current research interests include millimeter-wave beam steering antennas, such as lens antenna and antenna array.

MIKKO VARONEN received the M.Sc., Lic.Sc., and D.Sc. (Hons.) degrees in electrical engineering from Aalto University (formerly, Helsinki University of Technology), Espoo, Finland, in 2002, 2005, and 2010, respectively. In 2011, he was a NASA Postdoctoral Program Fellow with the Jet Propulsion Laboratory (JPL), California Institute of Technology (Caltech), Pasadena, CA, USA. In 2012, he was a Postdoctoral Researcher and the Academy of Finland Postdoctoral Researcher with the Department of Micro- and Nanosciences, Aalto University, from 2013 to 2016. During his Postdoctoral Fellowship, he was a Visiting Scientist with JPL, Electrical Engineering Department, Caltech, and the Fraunhofer Institute of Applied Solid-State Physics, Freiburg, Germany. He is currently a Senior Scientist and the Academy of Finland Research Fellow with the VTT Technical Research Centre of Finland, Espoo. His current research interests include the development of millimeter-wave integrated circuits using both silicon and compound semiconductor technologies for applications ranging from astrophysics and earth remote sensing to millimeter-wave communications.

MIKKO KAUNISTO was born in Inkoo, Finland, in 1963. He received the M.Sc. degree in physics from the University of Helsinki, Helsinki, Finland, in 2007. Since 2007, he has been a Research Scientist with the Antennas and RF Technologies Team, VTT Technical Research Centre of Finland, Espoo, Finland. His current research interest includes 3-D EM simulations from microwave up to terahertz frequencies.

ARTO RANTALA received the M.Sc. degree in power integrated circuits from the Tampere University of Technology (TTKK), in 1995. In his career, he has been a Lead Designer in several ASIC projects for EU, European Space Agency, and European industry. The design have been involved a wide range application of biosensor read-outs, data-converters, neural networks, and digital circuits. He has 38 reviewed articles and two patents related to a custom analog circuit design. His current research interests include the designing and specifying of mixed mode ASIC's and customizing the process design kits (PDK) for custom IC technologies.

MARKKU LAHTI received the M.Sc. and D.Sc. degrees in electrical engineering from the University of Oulu, Oulu, Finland, in 1993 and 2008, respectively. Since 2001, he has been with the VTT Technical Research Centre of Finland Ltd., Finland, where he is currently a Senior Scientist. He has authored or coauthored over 20 peer-reviewed publications and over 80 conference papers. He has been involved in several EU and ESA projects. His current research interests include the manufacturing of low-temperature co-fired ceramic substrates, module-level integration, and packaging of components with ceramic and polymer platforms.

ANTTI LAMMINEN received the M.Sc. and D.Sc.(Tech.) degrees in electrical engineering from Aalto University, Espoo, Finland, in 2006 and 2019, respectively. Since 2005, he has been a Research Trainee with the Antennas and RF Technologies Team, VTT Technical Research Centre of Finland, Espoo, where he has also been a Research Scientist, since 2006. He has over 40 publications (more than 800 citations) in journals and conference proceedings. His current research interests include beam-steerable millimetre-wave antennas and arrays, integration, and packaging of RF components from microwave up to terahertz frequencies. He is an Active Reviewer, for example, for IEEE Transactions on Antennas and Propagation, IEEE Antennas and Wireless Propagation Letters, and European Conference on Antennas and Propagation (EuCAP). He was a recipient of the 2017 EuMC Microwave Prize.

JAN HOLMBERG received the M.Sc. degree in electronics from Aalto University (formerly, Helsinki University of Technology), Espoo, Finland, in 1978. From 1977 to 1979, he has worked as a Research Engineer with the Acoustics Laboratory, Aalto University, and with Kari Pesonen Consulting Engineers, from 1980 to 1982, where he developing acoustic measuring systems. Since 1982, he has been a Research Scientist and a Senior Scientist with VTT Technical Research Centre of Finland Ltd., Espoo. He has been a Lecturer with the Circuit Theory Laboratory, Aalto University, where he teaching a senior/graduate level course on active filters, from 1985 to 2011. His recent research interests include design of millimeter wave integrated circuits and development of high speed communication systems. He is a member of the Audio Engineering Society, the Acoustical Society of Finland, and the Telecommunication and Electronics Association.

MIKKO KANTANEN received the M.Sc., Lic.Sc., and D.Sc. degrees in electrical engineering from Aalto University (formerly, Helsinki University of Technology), Espoo, Finland, in 2001, 2006, and 2017, respectively.

Since 2001, he has been working with MilliLab, VTT Technical Research Centre of Finland Ltd., Espoo, where he is currently a Senior Scientist. His research interests include millimeter-wave integrated circuit design, millimeter-wave measurements, and millimeter-wave systems.

Mr. Kantanen was a recipient of a 47th European Microwave Conference Microwave Prize and a co-recipient of an Asia-Pacific Microwave Conference 2006 Prize.

JUHA ALA-LAURINAHO received the Diploma Engineer (M.Sc.) degree in mathematics and D.Sc.(Tech.) degree in electrical engineering from Helsinki University of Technology (TKK), Finland, in 1995 and 2001, respectively.

He has been with TKK (currently Aalto University), serving with the Radio Laboratory, from 1995 to 2007; the Department of Radio Science and Engineering, from 2008 to 2016; and currently with the Department of Electronics and Nanoengineering. He also works as a Staff Scientist. He has been a Researcher and Project Manager in many millimeter wave technology related projects. His current research interests include the antennas and antenna measurement techniques for millimeter and submillimeter waves, and the millimeter wave imaging.

VILLE VIIKARI (Senior Member, IEEE) was born in Espoo, Finland, in 1979. He received the Master of Science (Tech.) and Doctor of Science (Tech.) (Hons.) degrees in electrical engineering from the Helsinki University of Technology (TKK), Espoo, in 2004 and 2007, respectively.

He is currently an Associate Professor and the Deputy Head of the Department with the Aalto University School of Electrical Engineering, Espoo. From 2001 to 2007, he was with the Radio Laboratory, TKK, where he studied antenna measurement techniques at submillimeter wavelengths and antenna pattern correction techniques. From 2007 to 2012, he was a Research Scientist and a Senior Scientist with the VTT Technical Research Centre, Espoo, where his research included wireless sensors, RFID, radar applications, MEMS, and microwave sensors. His current research interests include antennas for mobile networks, RF-powered devices, and antenna measurement techniques.

Dr. Viikari has served as the Chair for the Technical Program Committee of the ESA Workshop on Millimetre-Wave Technology and Applications and the Global Symposium on Millimeter Waves (GSMM), Espoo, in 2011 and 2016. He was a recipient of the Young Researcher Award of the Year 2014, presented by the Finnish Foundation for Technology Promotion, the IEEE Sensors Council 2010 Early Career Gold Award, the 2008 Young Scientist Award of the URSI XXXI Finnish Convention on Radio Science, Espoo, and the Best Student Paper Award of the annual symposium of the Antenna Measurement Techniques Association, Newport, RI, USA (October 30–November 4, 2005).